ELSEVIER

International Journal of Mass Spectrometry 205 (2001) 197–208

International Journal of Mass Spectrometry

# Very low energy electron scattering in nitromethane, nitroethane, and nitrobenzene

S.L. Lunt[a], D. Field[b,*], J.-P. Ziesel[c], N.C. Jones[d], R.J. Gulley[e,1]

[a]*Institute for Storage Ring Facilities, University of Århus, Ny Munkegade, DK-8000 Århus C, Denmark*
[b]*Institute of Physics and Astronomy, University of Århus, Ny Munkegade, DK-8000 Århus C, Denmark*
[c]*Laboratoire Collisions Agrégats Réactivité, Université Paul Sabatier, 31062 Toulouse, France*
[d]*Institute of Physics and Astronomy, University of Århus, Ny Munkegade, DK-8000 Århus C, Denmark and Department of Physics and Astronomy, University College London, Gower Street, London WC1E 6BT, UK*
[e]*School of Chemistry, University of Bristol, Bristol, BS8 1TS, UK*

Received 18 February 2000; accepted 8 August 2000

**Abstract**

Absolute total integral and total backward scattering cross sections are reported for $CH_3NO_2$, $C_2H_5NO_2$, and $C_6H_5NO_2$ at electron-impact energies from 30 meV to several eV, with some additional data at higher energies. These experimental data extend the range of species studied in low-energy electron scattering to include target molecules with dipole moments large enough to support dipole-bound states. Data provide a further test of the validity of the Born point-dipole approximation for the calculation of rotationally inelastic scattering cross sections for polar molecules, which are of importance in modeling the chemical and physical characteristics of industrial and natural plasmas. For $CH_3NO_2$ and $C_2H_5NO_2$, large cross sections are found, monotonically increasing with decreasing electron energy in qualitative and to some degree quantitative agreement with theory based on the Born model. As in earlier studies other polar species, the Born model is found to underestimate significantly backward-scattering cross sections. $C_6H_5NO_2$ shows a powerful dip in the total integral scattering cross sections $<$200 meV, a feature not found in the backward-scattering cross section and totally at variance with any simple theory. The suggestion is made that this behavior, in common with $ClO_2$ and $Cl_2O$, may arise through interference between direct Born-type rotational excitation and an indirect channel involving temporary negative ion states in the continuum. (Int J Mass Spectrom 205 (2001) 197–208) © 2001 Elsevier Science B.V.

*Keyword:* Electron-molecule interactions

## 1. Introduction

The subject of rotational excitation of polar molecules by low-energy electrons is one of considerable practical and theoretical interest. RF discharges used in the manufacturer of microelectronic devices frequently employ process gases that are polar species, for example, halogenated hydrocarbons. Rotationally inelastic scattering of electrons with these species and their reactive fragments occur with very large cross sections at low electron-impact energies. Rotationally inelastic collisions are a major factor in determining the electron temperature in RF plasmas. This in turn

* Corresponding author. E-mail: dfield@ifa.au.dk

[1] now at: AMPL, RSPhysSE, Australian National University, ACT 0200, Australia

Dedicated to Professor Aleksandar Stamatovic on the occasion of his 60th birthday.


*PII* S1387-3806(00)00376-6

influences potentials in the system, affecting the energy with which ions strike the substrate, a defining quantity in plasma manufacturing techniques [1,2]. Electron scattering cross sections for many species encountered in plasma chemistry, especially reactive fragments, cannot be studied in the laboratory. The predictive power of theory must therefore be tested on available experimental data so that theoretical values for other species may be used with confidence in plasma modeling. Inelastic scattering by polar molecules is also important in planetary atmospheres and in astrophysical plasmas. For example, collisions with CO [3] or with $H_2O$ in the interstellar medium contribute to the moderation of electron energies. This, in turn, will enhance the rate of recombination of electrons with molecular cations, the final stage in the production of the great majority of interstellar species.

The only general and readily accessible means of calculating cross sections for rotationally inelastic collisions of electrons with polar molecules is through use of the first-order Born point-dipole approximation. This method is conveniently simple to use, but it will fail if the electron energy is sufficiently low or if the dipole moment of the target is sufficiently high. The Born approximation is based on the assumption that many partial waves are involved in the scattering. At low-enough energy, contributions from higher partial waves must diminish in importance despite the long-range nature of the charge–dipole interaction. It is of considerable interest to determine the impact energy at which this breakdown of the Born approximation is significant. Turning to molecular targets with large dipole moments, it is well known that if the dipole exceeds ~2.5 D, then dipole-bound states may form [4,5]. Breakdown of the Born approximation for rotationally inelastic scattering has been observed at microvolt collision energies in experiments involving Rydberg atom collisions with polar species [6–8]. The suggestion is that dipole-bound states may be important in the scattering, especially if dipole-bound states act as a gateway to the formation of valence-negative ion states [9,10].

In this work we continue our studies of electron-impact rotational excitation of polar molecules [3,11–14], choosing target species of sufficiently high dipole moment that the influence of dipole-bound states may be apparent, namely, nitromethane, $CH_3NO_2$, 3.46 D; nitroethane, $C_2H_5NO_2$, 3.65 D; and nitrobenzene, $C_6H_5NO_2$, 4.23 D, where all dipole moments are taken from the CRC Handbook, 66th edition. Stockdale et al. [15], Compton et al. [9], and Gutsev and Bartlett [16] report experimental and theoretical studies of negative ion formation in Rydberg atom collisions with $CH_3NO_2$ and Frey et al. [6] and Desfrancois et al. [10] report similar experiments in $C_6H_5NO_2$. In $C_6H_5NO_2$, nondissociative electron attachment near zero energy has been observed with a lifetime of 17.5 $\mu$s for the metastable $C_6H_5NO_2^-$ ion [17,18]. Dissociative attachment in $C_6H_5NO_2$ to form $NO_2^-$ occurs at ~1.3 and ~3.6 eV [17,19].

There appear, however, to have been no detailed studies of low-energy electron scattering in any of the three species investigated here. To the best of the authors' knowledge, the only electron impact studies are those mentioned above for $C_6H_5NO_2$ and that of Flicker et al. [20], which involved electronic excitation in $CH_3NO_2$ in the 15- to 100-eV impact energy range. In this work, we have measured total integral and total backward-scattering cross sections in the energy range 30 meV to 2.5 eV for $CH_3NO_2$, 50 meV to 1.2 eV for $C_2H_5NO_2$, and 30 meV to ~10 eV for $C_6H_5NO_2$. Total integral cross sections include all elastic and inelastic events involving scattering into $4\pi$ steradians, so far as the geometry and potentials in the system allow. Total backward-scattering cross sections include all elastic and inelastic events leading to scattering only into the backward hemisphere between 90° and 180°. Tabulated data for the full energy ranges mentioned may be obtained on request.

## 2. Experimental method

The apparatus is described in detail previously [12,21] and is based on that described by Field et al. [22]. Electrons are formed by photoionization of Ar using focused monochromatized synchrotron radiation at the sharp autoionizing resonance Ar** $3p^5$ ($^2P_{1/2}$) 11s superposed on the broad 9d′ resonance at 78.65 nm [23], ~4 meV above the $^2P_{3/2}$ ionization

threshold. The experimental apparatus system consists of a photoionization region, electrostatic optics to convey electrons to a collision cell containing the target gas, and a channel electron multiplier for recording the electron current. The electron energy is controlled by varying the potential in the photoionization source. The whole system can be immersed in an axial magnetic field, which is typically set to 20 Gauss.

The experimental data reported here were all obtained at the ASTRID synchrotron (Institute for Storage Ring Facilities, University of Aarhus), save for the backward-scattering data for $C_6H_5NO_2$, which were obtained at the Daresbury Synchrotron Radiation Source (SRS). The total integral scattering cross section for $C_6H_5NO_2$ was measured on ASTRID using a beamline fitted with an undulator and a Miyake monochromator [24], working with a bandpass of ~0.45 Å. This yielded an effective energy resolution in the incident electron beam of 8 meV FWHM. Data for $CH_3NO_2$ and $C_2H_5NO_2$ were recorded on a newly commissioned spherical monochromator at the undulator beamline on the ASTRID synchrotron. This instrument was operated at a measured photon energy resolution of ~0.75 meV FWHM for total backward-scattering cross section measurements and ~1.5 meV FWHM for total integral cross sections. The work at the SRS used the VUV3.2 bending magnet beamline fitted with a 5-m McPherson normal incidence monochromator. This was used at a resolution of ~0.2 Å, equivalent to 3.5 meV FWHM [25].

The monochromator resolutions quoted above were in all cases determined from the observed form of threshold photoionization resonances in the spectrum of Ar. The energy distribution of the electrons is given by a convolution of the photon bandwidth of the ionizing radiation and the form of the combined 11-s resonance, of width 0.09 meV [26], and 9d′ resonance, of width ~6 meV. For the purposes of the present work, the energy resolution of the photoelectrons may be taken to be that of the photon bandwidth, as demonstrated in Field et al. [25]. We presently have no independent observations of very sharp electron-scattering features to confirm the higher resolution associated with the spherical grating monochromator on the ASTRID synchrotron.

The electrons are formed into a beam using a weak electrostatic draw-out field across the photoionization chamber. In the absence of a magnetic field, the draw-out field is typically 0.2 V/cm. In presence of the magnetic field, high draw-out efficiency may be achieved with lower electrostatic fields. In this work, draw-out fields of between a few mV and 120 mV/cm were used. The electron beam passes through a 1.8-mm aperture in the photoionization chamber and enters a system of electron optics, composed of a Calbick lens and a four-element electrostatic zoom lens. This serves to focus the electron beam into a field-free collision chamber of 30 mm length in which the target gas is contained. The diameter of the entrance aperture of the collision chamber is 2.0 mm and that of the exit aperture is 3.0 mm. Unscattered electrons are transported beyond the collision chamber via further optical elements and pass through a shielding mesh before detection at the channeltron.

Cross sections are measured through attenuation of the incident beam and evaluated using the Beer-Lambert law:

$$I(t) = I(0) \exp(-\sigma n l), \quad (1)$$

where $I(0)$ and $I(t)$ are the unattenuated and attenuated electron currents respectively, $\sigma$ is the scattering cross section (see below), $n$ is the target gas number density, and $l$ is the effective path length of electrons through the target gas. The pressure in the target cell was measured either with a Leybold rotating ball gauge (Viscovac VM212) or a capacitive manometer (Edwards 655).

Spectra were obtained by scanning the electron energy with dwell times at any energy of 1–2 s with a step size of typically 2 meV in the few hundred meV regime, rising to 5 or 10 meV at higher energies. Several spectra were summed to provide the data reported here. To obtain accurate values of scattering cross sections, experiments were also carried out at a variety of fixed electron-impact energies. For each energy, a succession of five pairs of measurements was performed, integrating the attenuated and unattenuated currents over a period of 120 s in each case. Account was taken of the slow decrease in time of the incident electron beam associated with the declining

current in the storage ring. The attenuation of the incident electron beam was maintained as low as possible, consistent with accurate pressure measurement. As cross sections are very high in the nitro-species studied here, attenuation was allowed in the worst case to rise to ~30%. However, a range of pressures was used to ensure that the derived cross sections were pressure independent and, thus, that multiple scattering did not make any appreciable contribution to the measurements.

In the absence of the magnetic field, the cross section obtained using Eq. (1) is the total integral cross section, $\sigma_t$, which will include attachment and dissociative attachment if present. In Eq. (1), the effective pathlength, $l$, of the electrons through the target gas is not necessarily the geometrical length of the cell. To obtain absolute values of cross sections, extensive experiments have been performed using $N_2$ with comparison of results in Sohn et al. [27] and Sun et al. [28]. These investigations show that in fact the geometrical length of the collision cell is an accurate measure of $l$. Details may be found in [14]. As discussed in Gulley et al. [12], the presence of a dipole moment in the target species causes significant systematic errors in measured total integral cross sections caused by strong forward scattering [29]. This is discussed further in section 3.1.

In the presence of the axial magnetic field, any electrons scattered into the forward hemisphere by the target gas are realigned to perform forward-moving helical trajectories around the axis of the field and are detected as unscattered. All electrons scattered in the backward hemisphere follow backward-moving trajectories around the direction of the magnetic field. These electrons are lost to the incident beam. The apparatus then determines cross sections for scattering between 90° and 180°, that is, total backward-scattering cross sections, $\sigma_b$, as defined in the introduction. Above a certain energy, in the presence of the magnetic field, electrons scattered at close to 90° will have sufficient transverse energy to cause them to move in a spiral path with a diameter such that they cannot pass through the exit hole of the target gas cell. For electrons on axis, this energy is ~800 meV, but the energy is lower for off-axis incident electrons. To determine the energy to which absolute backward-scattering cross sections are reliable, the backward cross section was measured in $N_2$ and compared with differential cross sections given in Sun et al. [28] integrated between 90° and 180°. Good agreement is found up to ~650 meV. The experimental technique for the determination of $\sigma_b$ has been very thoroughly checked in previous work (e.g., [13,14,30]).

An additional problem arises in the current work because, as noted above, attachment and dissociative attachment may take place when very low energy electrons encounter $CH_3NO_2$ [15] and $C_6H_5NO_2$ [6,10,17–19] and, very likely, also $C_2H_5NO_2$. The cross sections derived from Eq. (1) in the presence of a magnetic field cannot then be wholly associated with scattering into the angular range 90°–180° [21]. Nevertheless, for simplicity we continue to refer to cross sections measured in the presence of the magnetic field as backward-scattering cross sections, albeit including those regimes of energy in which electron attachment may participate in the scattering.

The absolute electron energy scale is calibrated by observing the peak in the $N_2^-\ ^2\pi_g$ resonance around 2.44 eV. Results in Rohr [31], Kennerley [32], and Randell et al. [30] indicate that the peak recorded in the total cross section at 2.440 eV is a good energy calibrator for both total and backward-scattering data and, thus, for experiments with and without the magnetic field present. We assign an energy of 2.442 eV to this peak, this figure being the average of the values of 2.440 and 2.444 eV in Kennerley [32] and Rohr [31], respectively. Agreement between the $N_2$ resonance energy and electron energies determined by the lens potentials typically lay between 10 and 50 meV and did not vary significantly over the course of many experiments. We estimate that the absolute energy scale in the present data is accurate to ±5 meV.

## 3. Results and discussion

### 3.1. $CH_3NO_2$ and $C_2H_5NO_2$

Total integral and backward-scattering transmission spectra for $CH_3NO_2$ and $C_2H_5NO_2$ are shown in

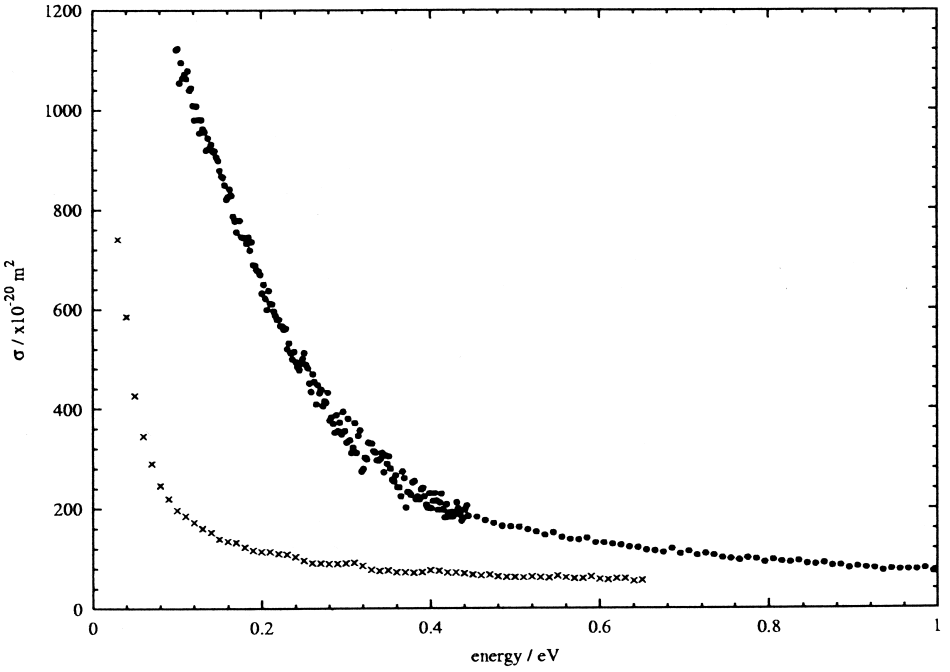


Fig. 1. Total integral-scattering cross sections for $CH_3NO_2$ (upper set of points) and backward-scattering cross sections for $CH_3NO_2$ (lower set of points) versus electron impact energy between 30 meV and 1 eV.

Figs. 1 and 2. The cross sections are strongly dominated by rotationally inelastic scattering at the electron-impact energies shown. Salient features are the sharp rise in scattering cross section at low energies and strong forward scattering. This behavior of the cross section is in qualitative agreement with the predictions of the Born point-dipole model. For all three species, the contribution to the total scattering cross sections from elastic scattering is unlikely to exceed a few tens of $Å^2$ throughout the energy range considered [33], and elastic scattering is therefore ignored in the subsequent discussion. The quadrupole moments of the molecules studied here are not known. If it is assumed that their absolute values lie in the expected range of a few a.u., quadrupole-scattering cross sections may be shown not to exceed more than a few $Å^2$ at any electron-impact energy of interest here [3,34].

To examine the quantitative accuracy of the Born model, we now compare our experimental results in the low-energy regime with the predictions of the first Born point-dipole approximation for rotational excitation. The theory of rotational excitation of molecules by slow electrons has been reviewed by Takayanagi [35] and references therein. Our analysis is based on Crawford [36], who derived expressions for the scattering of electrons from polar symmetric top molecules. Spectroscopic data for $CH_3NO_2$ [37] and $C_2H_5NO_2$ [38] show that the corresponding asymmetry parameters, $\kappa$ ($=[2B - A - C]/[A - C]$), are 0.25 and $-0.69$ respectively. For simplicity, $CH_3NO_2$ was treated as an oblate symmetric top and $C_2H_5NO_2$ as a prolate symmetric top. The pure rotational scattering cross section in SI units between the rotational levels $(J, K)$ and $(J', K')$ integrated between the two angles $\theta_1$ to $\theta_2$ may be expressed as

$$\sigma(J,K;J',K') = \xi(2J+1)\begin{pmatrix} J & J' & 1 \\ K & -K' & 0 \end{pmatrix}^2 \times \ln\left[\left|\frac{(k^2+k'^2-2kk'\cos\theta_2)}{(k^2+k'^2-2kk'\cos\theta_1)}\right|^{1/2}\right], \quad (2)$$

where $\xi = (4\pi/3k^2)(\mu^2/[ea_0]^2)$.

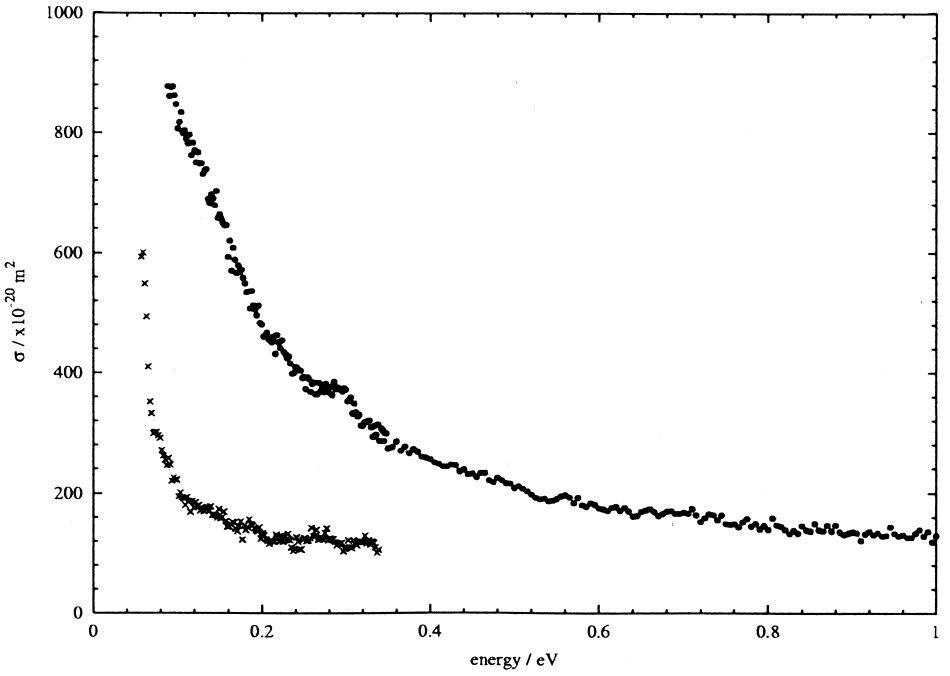


Fig. 2. Total integral-scattering cross sections for $C_2H_5NO_2$ (upper set of points) and backward-scattering cross sections for $C_2H_5NO_2$ (lower set of points) versus electron impact energy between 60 meV and 1 eV.

In Eq. (2), $J$ is the total angular momentum quantum number of the free molecule and $K$ is its effective projection on the molecular axis in symmetric top terms. $k'$ and $k$ are the magnitudes of the final and initial wavevectors given by $k = (2m_eE)^{1/2}/\hbar$, where $m_e$ and $E$ are the mass and energy of the electron, $ea_0 = 8.4784 \times 10^{-30}$ Cm and $\mu$ is the dipole moment of the target molecule expressed in centimeters. The Wigner 3-j symbols in Eq. (2) are evaluated using the tables given in Mizushima [39].

To simulate the rotationally inelastic contribution to the experimental scattering spectra, the Boltzmann populations of the target molecular rovibrational levels must be calculated. Vibrationally excited levels were included up to an energy of 1000 $cm^{-1}$. For $CH_3NO_2$, this involved populations of levels with one quantum of the $NO_2$ symmetric bend, the C–N stretch, the $NO_2$ ($B_2$) rock and two quanta of the $NO_2$ ($B_1$) rock [40]. For $C_2H_5NO_2$, levels with one quantum of $NO_2$ symmetric bend and C–N stretch and two quanta of $NO_2$ rock were included [40]. Vibrationally inelastic scattering is not, however, included, as it is of low cross section compared with rotationally inelastic scattering.

The energies of rotational levels were calculated using standard formulae for prolate and oblate tops, taking averages of the B and C rotational constants (see, e.g., [12]). We use selection rules appropriate for symmetric tops implicit in Eq. (2), namely $\Delta J = 0$, $\pm 1$, and $\Delta K = 0$. Spectra are simulated by combining at any energy all contributions from rotationally inelastic events, folding in the appropriate gaussian energy distribution for the incident electrons. In performing this analysis, we have, for simplicity, ignored degeneracy splitting caused by internal rotation and, also, effects of nuclear statistics.

The geometry of the collision chamber dictates that we omit to record a part of the cross section associated with low-angle scattering, as noted in the Experiment & Method Section. The problem of the nondetection of forward scattering has been dealt with at some length in Floeder et al. [29]. We follow the method used in that paper to calculate the effective rotationally inelastic Born cross sections. Thus, to compare

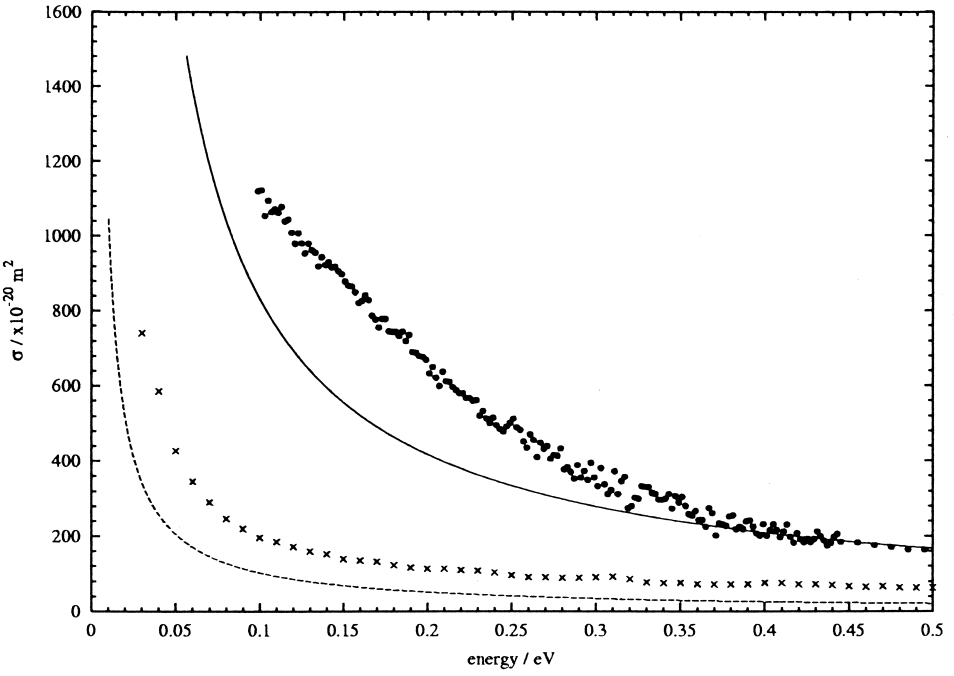


Fig. 3. Predictions of the Born theory for integral rotationally inelastic scattering (upper solid line) and for backward rotationally inelastic scattering (lower dashed line) compared with experimental data for $CH_3NO_2$.

the predictions of the Born theory with experimental results, theoretical values are estimated from Eq. (2), using a range of values of $\theta_1$, appropriate to the cell length of 30 mm and exit-hole diameter of 3 mm. We use a coarse numerical integration over the distance along the collision chamber, for each distance using an appropriate value of angle $\theta_1$, with $\theta_2 = 180°$, referring to Eq. (2). This corrected cross section may be expressed as $l^{-1} \int_0^l dl\, [\sigma_{Born}]_{\theta_1}^{2\pi}$, where $\sigma_{Born}$ is the cross section calculated from Born theory for on-axis electrons for the appropriate value of $l$ (which dictates the value of $\theta_1$). We have used more values of $\theta_1$ between 3° and 27°, corresponding to a set of equidistant points along the collision chamber. All calculations of the Born scattering cross section reported here involve this effective reduction in the full angular range.

Fig. 3 and Fig. 4 show, respectively, the Born theory predictions superimposed on our experimental data. The extent of agreement between theory and experiment adds weight to the conclusion emerging from a number of recent experiments that the Born point-dipole approximation is reliable at energies of a few hundred meV but that significant discrepancies may arise at lower energies. The Born model may underestimate the scattering cross section at low-impact energy, as in the present work for $CH_3NO_2$ and in the halobenzenes [13], or it may provide an overestimate, as in ozone [12].

A clear trend in all cases, reinforced by data reported here, is that the Born model underestimates the backward-scattering cross section: see lower pairs of curves in Figs. 3 and 4. As discussed in Lunt et al. [13], the Born model is based on the assumption that the long range of the electron–dipole potential has the result that very many partial waves are involved in the scattering. Thus, in the Born model, high angular momentum collisions suffer weak interactions and cause little deviation in the direction of the impinging wave. The electrons are, therefore, strongly forward scattered. Individual partial wave phase shifts are small, in the sense that $\sin(\eta_l) \sim \eta_l$. At sufficiently low energy, this model must break down, as high $l$ waves concentrate increasingly far from the target as

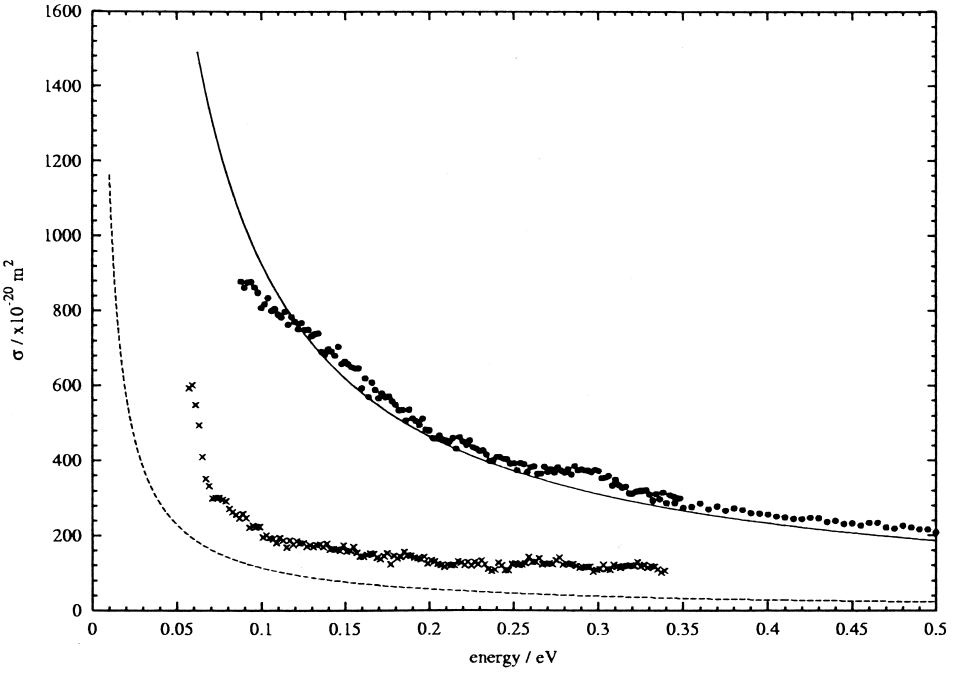


Fig. 4. Predictions of the Born theory for total integral rotationally inelastic scattering (upper solid line) and for backward rotationally inelastic scattering (lower dashed line) compared with experimental data for $C_2H_5NO_2$.

the $k$ vector falls. In a real system, the proportion of backward scattering therefore exceeds that calculated using the Born model, as lower partial waves make a greater contribution and individual partial waves suffer greater phase shifts.

In the total integral scattering data for $C_2H_5NO_2$ in Fig. 2, there is a small feature with a threshold at ~280 meV and maximum cross section relative to a smoothly varying background of ~30 Å$^2$. The value of the threshold energy is not characteristic of any IR active vibrational frequencies in $C_2H_5NO_2$, and this feature cannot, therefore, be ascribed to threshold vibrational excitation. We tentatively ascribe this peak to dissociative attachment, presumably to form $NO_2^-$, by analogy with dissociative attachment (DA) in $CH_3NO_2$ at 600 meV [15]. The DA process in $CH_3NO_2$ is apparently of too low cross section to be detectable in the present experiment. Returning to the small peak in the total integral scattering cross section in $C_2H_5NO_2$, this was not observed within the signal-to-noise ratio in the backward-scattering cross section. In $CH_3NO_2$, the lowest unoccupied molecular orbital (LUMO) is $b_1$ [41]. To a good approximation, the nature of the LUMO in $C_2H_5NO_2$ is dictated by the $NO_2$ group and is little affected by the substitution of an ethyl for a methyl group in $C_2H_5NO_2$. Given that the LUMO of $C_2H_5NO_2$ may be approximately characterized as a $b_1$ orbital, attachment should be through $p$ waves (and higher waves of odd $l$; see section 3.2), as the $l = 1$ spherical harmonics transform as $B_1$ under the operations of the $C_{2v}$ local symmetry. Attachment by $p$ waves may have strong backward–forward asymmetry and could explain the absence of any discernible feature in the backward-scattering cross section. Similar behavior is found in proposed $p$-wave attachment to $OClO$, for which structure in the integral-scattering cross section is considerably more marked than in the backward-scattering cross section [14].

### 3.2. $C_6H_5NO_2$

Total integral- and backward-scattering transmission spectra for $C_6H_5NO_2$ are shown in Fig. 5. Data

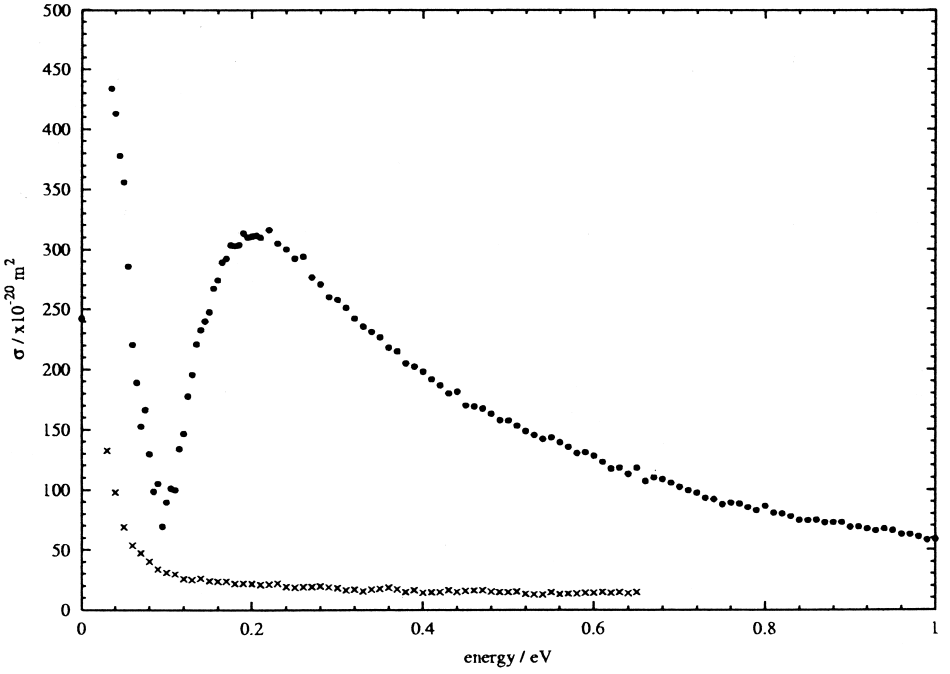


Fig. 5. Total integral-scattering cross sections for $C_6H_5NO_2$ (upper set of points) and backward-scattering cross sections for $C_6H_5NO_2$ (lower set of points) versus electron impact energy between 30 meV and 1 eV.

above 1 eV (available on request) show a weak feature around 3.75 eV, which may be associated with dissociative attachment [17,19]. No structure can, however, be discerned around 1.3 eV, where dissociative attachment has also been observed to take place [17,19]. This feature is presumably obscured by the falling nonresonant background in our data in this energy regime.

In the range of energy down to ~250 meV, data in Fig. 5 show the scattering behavior expected of a molecule with a large dipole moment, that is, a monotonic rise in cross section to a value of several hundred Å$^2$ with strong forward scattering. The rotationally inelastic scattering spectrum was calculated for $C_6H_5NO_2$ using the formalism of the previous section. The asymmetry parameter is −0.796 [42], and the molecule was treated as a prolate symmetric top. Vibrational populations included levels up to $v = 3$ for the 176-cm$^{-1}$ mode, $v = 2$ for modes at 252 and 397 cm$^{-1}$ and $v = 1$ at 420 cm$^{-1}$ involving C–C bending, $NO_2$ rocking, and C–N stretching [43,44]. For comparison with experimental data, the elastic contribution to the scattering is ignored, as in section 3.1. Results of the Born analysis show that the model overestimates the cross section by ~50% at 500 meV electron-impact energy. The Born model also predicts a more rapid rise in rotationally inelastic scattering than is observed in the 500 to ~250 meV energy range. Beyond this energy, the integral cross section falls sharply in a manner completely at variance with any simple model. At the lowest-impact energy investigated of 35 meV, the total integral cross section remains an order of magnitude below that predicted by the Born model for rotationally inelastic scattering. By contrast, the backward-scattering cross section shows monotonic behavior and behaves qualitatively in accord with the Born model. Backward scattering cross sections are, however, a factor of ~5 below that predicted by Born at the lowest energies used. Comparison between experimental results and predictions of the Born model are shown in Fig. 6.

The strong suppression of rotational excitation in $C_6H_5NO_2$ at energies <200 meV must arise through an interference phenomenon in which incoming and

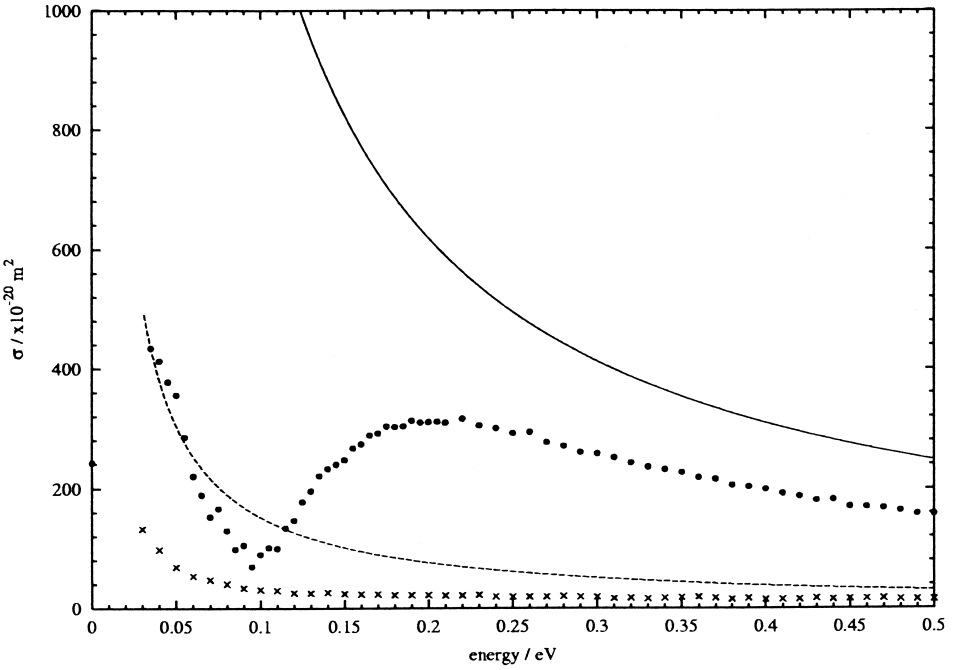


Fig. 6. Predictions of the Born theory for integral rotationally inelastic scattering (upper solid line) and for backward rotationally inelastic scattering (lower dashed line) compared with experimental data for $C_6H_5NO_2$.

outgoing waves, scattered through rotationally inelastic events, destructively interfere. This is reminiscent of the Ramsauer-Townsend effect. The latter, however, takes place only in the *s* wave. Here we seek a phenomenon that affects higher partial waves, as these are important in rotationally inelastic scattering. In addition, the data show strongly anisotrophic effects, indicating the involvement of higher partial waves. We suggest that $C_6H_5NO_2$ displays interference between the direct rotationally inelastic scattering channel and an indirect scattering channel via $C_6H_5NO_2^-$ states embedded in the continuum. An analogy may clearly be drawn with Fano-type phenomena.

Indeed, the dependence of the cross section on electron energy has some of the character of a Fano line profile. The LUMO of $C_6H_5NO_2$ is $b_1$ and, as in $CH_3NO_2$ and $C_2H_5NO_2$, attachment to form a temporary negative ion is allowed by $l = 1, 3, 5, 7 \ldots$ partial waves. As in the Born model, individual partial waves contribute weakly, leading to an interference effect seen only in the forward hemisphere. It has been suggested that dipole-bound states may act as doorway states to valence bound negative ion states of $C_6H_5NO_2$ [10]. This channel may allow $l = 0, 2, 4, 6 \ldots$ to participate in the scattering via dipole state formation and coupling through the dipole part of the nuclear kinetic energy operator to form $C_6H_5NO_2^-$. In this connection, the formation of $C_6H_5NO_2^-$ involves large structural changes in the nuclear framework [10].

## 4. Concluding remarks

Few general conclusions may at present be drawn about the validity of the first-order Born point-dipole model, despite the accumulating quantity of data for low-energy scattering by polar models. The Born model appears to have a range of validity within an error of a few tens of percent in the range of electron impact energy >200 meV. At lower energies, this level of agreement may not be maintained. The

forward–backward asymmetry of the scattering is always exaggerated in the model, and this may be readily understood on the basis of the breakdown of assumptions in the Born model.

There is a set of species, presently including $ClO_2$ [14], $Cl_2O$ (unpubl.) and $C_6H_5NO_2$, for which the variation of cross section at energies around 250 meV and below shows marked structure. This structure is not understood, and no theoretical studies are yet available. Its presence has the effect that species become relatively transparent to electrons in certain ranges of very low energy. This would clearly have consequences for calculations of the low-energy tail of the electron energy distribution in a low-pressure plasma. The molecules in question have their display of temporary negative ion formation at low energy in common with $C_6H_5NO_2$ possessing dipole-bound states. The suggestion is that interference may occur between direct rotational excitation and indirect excitation via temporary negative ion states, giving rise to a drop in scattering cross section where a rapid rise is predicted by the Born model. This remains, however, only a conjecture and begs the question of why $CH_3NO_2$ and $C_2H_5NO_2$ do not also show this behavior.

## Acknowledgements

We thank the directors and staff both of the Institute of Storage Ring facilities at the University of Aarhus (ISA) and the Daresbury Synchrotron Radiation Source for their provision of synchrotron radiation facilities on ASTRID and the SRS. J.P.Z. gratefully acknowledges financial support from the Royal Society (UK), CNRS (France), and SNF (Denmark) under European Science Exchange programs.

## References

[1] D. Field, D.F. Klemperer, P.W. May, Y.P. Song, J. Appl. Phys. 70 (1991) 82.
[2] Y.P. Song, D. Field, D.F. Klemperer, J. Phys. D: Appl. Phys. 23 (1990) 673.
[3] J. Randell, R.J. Gulley, S.L. Lunt, J.-P. Ziesel, D. Field, J. Phys. B: At. Mol. Opt. Phys. 29 (1996) 2049.
[4] C. Desfrancois, H. Abdoul-Carime, N. Khelifa, J.-P. Schermann, Phys. Rev. Lett. 73 (1994) 2436.
[5] G.L. Gutsev, L. Adamowicz, J. Phys. Chem. 99 (1995) 13412.
[6] M.T. Frey, S.B. Hill, X. Ling, K.A. Smith, F.B. Dunning, Phys. Rev. A. 50 (1994) 3124.
[7] X. Ling, K.A. Smith, F.B. Dunning, Phys. Rev. A47 (1993) R1.
[8] X. Ling, M.T. Frey, K.A. Smith, F.B. Dunning, Phys. Rev. A48 (1993) 1252.
[9] R.N. Compton, H.S. Carman, C. Desfrancois, H. Abdoul-Carime, J.P. Schermann, J.H. Hendricks, S.A. Lyapustina, K.H. Bowen, J. Chem. Phys. 105 (1996) 3472.
[10] C. Desfrancois, V. Périquet, S.A. Lyapustina, T.P. Lippa, D.W. Robinson, K.H. Bowen, H. Nonaka, R.N. Compton, J. Chem. Phys. 111 (1999) 4569.
[11] J. Randell, J.-P. Ziesel, S.L. Lunt, G. Mrotzek, D. Field, J. Phys. B: At. Mol. Opt. Phys. 26 (1993) 3423.
[12] R.J. Gulley, T.A. Field, W.A. Steer, N.J. Mason, S.L. Lunt, J.-P. Ziesel, D. Field, J. Phys. B: At. Mol. Opt. Phys. 31 (1998) 5197.
[13] S.L. Lunt, D. Field, S.V. Hoffman, R.J. Gulley, J.-P. Ziesel, J. Phys. B: At. Mol. Opt. Phys. 32 (1999) 2707.
[14] D. Field, N.C. Jones, J.M. Gingell, N.J. Mason, S.L. Lunt, J.-P. Ziesel, J. Phys. B: At. Mol. Opt. Phys. 33 (2000) 1039.
[15] J.A. Stockdale, F.J. Davis, R.N. Compton, C.E. Klots, J. Chem. Phys. 60 (1974) 4279.
[16] G.L. Gutsev, R.J. Bartlett, J. Chem. Phys. 105 (1996) 8785.
[17] L.G. Christophorou, R.N. Compton, G.S. Hurst, P.W. Reinhardt, J. Chem. Phys. 45 (1966) 536.
[18] W.T. Naff, R.N. Compton, C.D. Cooper, J. Chem. Phys. 54 (1971) 212.
[19] R.N. Compton, R.H. Huebner, P.W. Reinhardt, L.G. Christophorou, J. Chem. Phys. 48 (1968) 901.
[20] W.M. Flicker, O.A. Mosher, A. Kuppermann, Chem. Phys. Lett. 60 (1979) 518.
[21] R.J. Gulley, S.L. Lunt, J.-P. Ziesel, D. Field, J. Phys. B: At. Mol. Opt. Phys. 31 (1998) 2735.
[22] D. Field, D.W. Knight, S.L. Lunt, G. Mrotzek, J.-B. Ozenne, J.-P. Ziesel, Meas. Sci. Technol. 2 (1991) 757.
[23] K. Radler, J. Berkowitz, J. Chem. Phys. 70 (1979) 221.
[24] M. Howells, D. Norman, G.P. Williams, J.B. West, J. Phys. E: Sci. Instrum. 11 (1978) 199.
[25] D. Field, G. Mrotzek, D.W. Knight, S.L. Lunt, J.-P. Ziesel, J. Phys. B: At. Mol. Opt. Phys. 21 (1988) 171.
[26] D. Klar, K. Harth, J. Ganz, T. Kraft, M.-W. Ruf, H. Hotop, V. Tsemekhman, K. Tsemekhman, M. Ya. Amusia, Z. Phys. D 23 (1992) 101.
[27] W. Sohn, K.-H. Kochem, K. Jung, H. Ehrhardt, J. Phys. B: At. Mol. Opt. Phys. 19 (1986) 4017.
[28] W.G. Sun, M.A. Morrison, W.A. Isaacs, W.K. Trail, D.T. Alle, R.J. Gulley, M.J. Brennan, S.J. Buckman, Phys. Rev. A52 (1995) 1229.
[29] K. Floeder, D. Fromme, W. Raith, A. Schwab, G. Sinapius, J. Phys. B: At. Mol. Opt. Phys. 18 (1985) 3347.
[30] J. Randell, S.L. Lunt, G. Mrotzek, J.-P. Ziesel, D. Field, J. Phys. B: At. Mol. Opt. Phys. 27 (1994) 2369.
[31] K. Rohr, J. Phys. B: At. Mol. Opt. Phys. 10 (1977) 2215.

[32] R.E. Kennerly, Phys. Rev. A21 (1980) 1876.
[33] S.L. Lunt, J. Randell, J.-P. Ziesel, G. Mrotzek, D. Field, J. Phys. B: At. Mol. Opt. Phys. 31 (1998) 4225.
[34] E. Gerjuoy, S. Stein, Phys. Rev. 97 (1955) 1671.
[35] K. Takayanagi in I. Shimamura and K. Takayanagi, eds. Electronic and Atomic Collisions. Plenum, New York, 1984.
[36] O.H. Crawford, J. Chem. Phys. 47 (1967) 1100.
[37] F. Rohart, J. Mol. Spectroscopy 57 (1975) 301.
[38] Krishnaji, G.K. Pandet, Ind. J. Pure. App. Phys. 8 (1970) 261.
[39] M. Mizushima, Quantum mechanics of atomic spectra and atomic structure (1970), Benjamin, New York.
[40] D.C. Smith, C.-Y. Pan, J.R. Nieslen, J. Chem. Phys. 18 (1950) 706.
[41] J.W. Rabalais, J. Chem. Phys. 57 (1972) 960.
[42] K.E. Reinert, Z. Naturf. A15 (1960) 85.
[43] E.B. Wilson, Phys. Rev. 45 (1934) 706.
[44] J.H.S. Green, W. Kynaston, A.S. Lindsey, Spectrochim. Acta 17 (1961) 486.